arXiv:1403.5481v2 [stat.AP] 4 May 2015

Assessment of the lognormality assumption of seismic fragility curves using non-parametric representations

B. Sudret[a], C. Mai[a], K. Konakli[a,*]

[a]*ETH Zürich, Institute of Structural Engineering, Chair of Risk, Safety & Uncertainty Quantification, Stefano-Franscini-Platz 5, CH-8093 Zürich, Switzerland*

Abstract

Fragility curves are commonly used in civil engineering to estimate the vulnerability of structures to earthquakes. The probability of failure associated with a prescribed criterion (e.g. the maximal inter-storey drift ratio exceeding a prescribed threshold) is represented as a function of the intensity of the earthquake ground motion (e.g. peak ground acceleration or spectral acceleration). The classical approach consists in assuming a lognormal shape of the fragility curves. In this paper, we introduce two non-parametric approaches to establish the fragility curves without making any assumption, namely the binned Monte Carlo simulation approach and kernel density estimation. As an illustration, we compute the fragility curves of a 3-storey steel structure, accounting for the nonlinear behavior of the system. The curves obtained with the proposed approaches are compared with each other and with those obtained using the classical lognormal assumption. It is shown that the lognormal curves differ significantly from their non-parametric counterparts.

Keywords: earthquake engineering, fragility curves, lognormal assumption, non-parametric approach, kernel density estimation, epistemic uncertainty

1. Introduction

The severe socio-economic consequences of several recent earthquakes highlight the need for proper seismic risk assessment as a basis for efficient

*Corresponding author
Email address: konakli@ibk.baug.ethz.ch (K. Konakli)
URL: www.ibk.ethz.ch/su/people/sudretb/index_EN (B. Sudret)

decision making on mitigation actions and disaster planning. To this end, the probabilistic performance-based earthquake engineering (PBEE) framework has been developed, which allows explicit evaluation of performance measures that serve as decision variables (DV) (*e.g.* monetary losses, casualties, downtime) accounting for all prevailing uncertainties (*e.g.* characteristics of ground motions, structural properties, damage occurrence). The key steps in the PBEE framework comprise the identification of seismic hazard, evaluation of structural response, damage analysis and eventually, consequence evaluation. In particular, the mean annual frequency of exceedance of a DV is evaluated as [1, 2, 3]:

$$\lambda(DV) = \int\int\int P(DV|DM)\,\mathrm{d}P(DM|EDP)\,\mathrm{d}P(EDP|IM)\,\mathrm{d}\lambda(IM) \quad (1)$$

in which $P(x|y)$ is the conditional probability of x given y, DM is a damage measure typically defined according to repair costs (*e.g.* light, moderate or severe damage), EDP is an engineering demand parameter obtained from structural analysis (*e.g.* force, displacement, drift ratio), IM is an intensity measure characterizing the ground motion severity (*e.g.* peak ground acceleration, spectral acceleration) and $\lambda(IM)$ is the annual frequency of exceedance of the IM. Determination of the probabilistic model $P(EDP|IM)$ constitutes a major challenge in the PBEE framework since the earthquake excitation contributes the most significant part to the uncertainty in the DV. This step of the analysis is the focus of the present paper.

The conditional probability $P(EDP \geq \overline{edp}|IM)$, where $\overline{edp}$ denotes an acceptable demand threshold, is commonly represented graphically in the shape of the so-called demand fragility curves [4]. Thus, a demand fragility curve represents the probability that an engineering demand parameter exceeds a prescribed threshold as a function of an intensity measure of the earthquake motion. For the sake of simplicity, demand fragility curves are simply denoted fragility curves in the following analysis, which is also typical in the literature see *e.g.* [5, 6]. We note however that in other publications the term *fragility* is also used for $P(DM \geq \overline{dm}|IM)$ and $P(DM \geq \overline{dm}|EDP)$, *i.e.* the conditional probability of damage exceeding a threshold $\overline{dm}$ given the intensity measure [7] or the engineering demand parameter [2, 3], respectively.

Originally introduced in the early 1980's for nuclear safety evaluation [8], fragility curves are nowadays widely used for multiple purposes, *e.g.* seismic loss estimation [9], estimation of the collapse risk of structures in seismic

regions [10], design checking process [11], evaluation of the effectiveness of retrofit measures [12], etc. It is noteworthy that novel methodological contributions to fragility analysis have been made in recent years, including the development of multi-variate fragility functions [13], incorporation of Bayesian updating [14] and time-dependent fragility curves [15]. However, the classical fragility curves remain a popular tool in seismic risk assessment and recent literature is rich with applications on various type of structures, such as irregular buildings [6], underground tunnels [16], a pile-supported wharf [17], wind turbines [18], nuclear power plant equipments [19]. The estimation of such curves is the focus of this paper.

Fragility curves are typically classified into four categories according to the data sources, namely analytical, empirical, judgment-based or hybrid fragility curves [20]. Analytical fragility curves are derived from data obtained by analyses of structural models. Empirical fragility curves are based on the observation of earthquake-induced damage reported in post-earthquake surveys. Judgment-based curves are estimated by expert panels specialized in the field of earthquake engineering. Hybrid curves are typically obtained by combining data from different sources. Each category of fragility curves has its own advantages as well as drawbacks. In this paper, analytical fragility curves established using data collected from numerical structural analyses are of interest.

The typical approach to compute analytical fragility curves presumes that the curves have the shape of a lognormal cumulative distribution function [21, 22]. This approach is therefore considered *parametric*. The parameters of the lognormal distribution are determined either by maximum likelihood estimation [21, 23, 13] or by fitting a linear probabilistic seismic demand model in the log-scale [5, 24, 25, 26]. The assumption of lognormal fragility curves is almost unanimous in the literature due to the computational convenience as well as due to the facility for combining such curves with other elements of the seismic probabilistic risk assessment framework. However, the validity of such assumption remains questionable.

In the present work, we present two novel non-parametric approaches to establish the fragility curves without making any assumption, namely the binned Monte Carlo simulation (bMCS) and kernel density estimation (KDE). The main advantage of bMCS over traditional Monce Carlo simulation approaches ([27, 28]) is that it avoids the bias induced by scaling ground motions to predefined intensity levels. In the KDE approach, we introduce a statistical methodology for fragility estimation, which also opens new paths

for estimation of multi-dimensional fragility functions. The proposed methods are subsequently used to investigate the validity of the lognormal assumption in a case study where we develop fragility curves for different thresholds of the maximum inter-storey drift ratio of an example building structure. The proposed methodology can be applied in a straightforward manner to other types of structures or classes of structures or using different failure criteria.

The computation of fragility curves requires a sufficiently large number of transient dynamic analysis of the structure under seismic excitations that are either recorded or synthetic. Due to the lack of recorded signals with the properties of interest (*e.g.* earthquake magnitude, duration, etc.), it is common practice to generate suitable samples of synthetic ground motions [29, 12].

The paper is organized as follows: in Section 2, the method recently proposed by [30] to generate synthetic earthquakes, used in the example in Section 4, is briefly recalled. This method is selected because it allows to account for uncertainty in the intensity level of the motions for a given earthquake scenario. The different approaches for establishing the fragility curves, namely the classical lognormal, bMCS and KDE approaches, are presented in Section 3. In Section 4, we compute the fragility curves of a steel frame structure subject to seismic excitations using the aforementioned approaches and compare the results.

2. Recorded and synthetic ground motions

2.1. Recorded ground motions: notation

Let us consider a recorded earthquake accelerogram $a(t)$, $t \in [0, T]$ where T is the total duration of the motion. The peak ground acceleration reads: $PGA = \max_{t\in[0,T]} |a(t)|$. The Arias intensity I_a is defined by:

$$I_a = \frac{\pi}{2g} \int_0^T a^2(t)\, \mathrm{d}t \tag{2}$$

Defining the cumulative square acceleration by:

$$I(t) = \frac{\pi}{2g} \int_0^t a^2(\tau)\, \mathrm{d}\tau\,, \tag{3}$$

one defines the time instant t_α by:

$$t_\alpha : \qquad I(t_\alpha) = \alpha I_a \qquad \alpha \in [0,1] \tag{4}$$

Remarkable properties of a recorded seismic motion are the duration of the *strong motion phase* $D_{5-95} = t_{95\%} - t_{5\%}$ and the instant at the middle of the strong-shaking phase $t_{mid} \equiv t_{45\%}$.

2.2. Simulation of synthetic ground motions

For the sake of completeness, we summarize in this section the parameterized approach proposed by [30] in order to simulate synthetic ground motions. The seismic acceleration $a(t)$ is represented as a non-stationary process. Der Kiureghian and Rezaeian separate the non-stationarity into two components, namely a spectral and a temporal one, by means of a modulated filtered Gaussian white noise:

$$a(t) = \frac{q(t,\boldsymbol{\alpha})}{\sigma_h(t)} \int_0^t h\left[t-\tau, \boldsymbol{\lambda}\left(\tau\right)\right] \omega(\tau)\, \mathrm{d}\tau \tag{5}$$

in which $q(t,\boldsymbol{\alpha})$ is the deterministic non-negative *modulating function*, the integral is the non-stationary response of a linear filter subject to a Gaussian white noise excitation and $\sigma_h(t)$ is the standard deviation of the response process. The Gaussian white-noise process denoted by $\omega(\tau)$ will pass through a filter $h\left[t-\tau, \boldsymbol{\lambda}(\tau)\right]$ which is selected as the pseudo-acceleration response of a single-degree-of-freedom (SDOF) linear oscillator:

$$\begin{aligned} &h\left[t-\tau, \boldsymbol{\lambda}(\tau)\right] = 0 \quad \text{for} \quad t < \tau \\ &h\left[t-\tau, \boldsymbol{\lambda}(\tau)\right] = \frac{\omega_f(\tau)}{\sqrt{1-\zeta_f^2(\tau)}} \exp\left[-\zeta_f(\tau)\omega_f(\tau)(t-\tau)\right] \sin\left[\omega_f(\tau)\sqrt{1-\zeta_f^2(\tau)}(t-\tau)\right] \\ &\qquad\qquad \text{for} \quad t \geq \tau \end{aligned} \tag{6}$$

where $\boldsymbol{\lambda}(\tau) = (\omega_f(\tau), \zeta_f(\tau))$ is the vector of time-varying parameters of the filter h. Note that $\omega_f(\tau)$ and $\zeta_f(\tau)$ are the filter's natural frequency and damping ratio at instant τ, respectively. They are related to the evolving predominant frequency and bandwidth of the ground motion that is to be represented. The statistical analysis of real signals shows that $\zeta_f(\tau)$ may

be taken as a constant ($\zeta_f(\tau) \equiv \zeta$) while the predominant frequency varies approximately linearly in time [31]:

$$\omega_f(\tau) = \omega_{mid} + \omega'(\tau - t_{mid}) \tag{7}$$

In Eq. (7) t_{mid} is the instant at which 45% of the Arias intensity I_a is reached, $\omega_{mid} = \omega_f(t_{mid})$ is the filter's frequency at instant t_{mid} and ω' is the slope of the linear evolution. After being normalized by the standard deviation $\sigma_h(t)$, the integral in Eq. (5) becomes a unit variance process with time-varying frequency and constant bandwidth. The non-stationarity in intensity is then captured by the modulating function $q(t, \boldsymbol{\alpha})$. This time-modulating function determines the shape, intensity and duration T of the signal. A Gamma-like function is typically used [31]:

$$q(t, \boldsymbol{\alpha}) = \alpha_1 t^{\alpha_2 - 1} \exp(-\alpha_3 t) \tag{8}$$

where $\boldsymbol{\alpha} = \{\alpha_1, \alpha_2, \alpha_3\}$ is directly related to the energy content of the signal through the quantities I_a, D_{5-95} and t_{mid} defined in Section 2.1, see [31] for details. For computational purposes, the acceleration in Eq. (5) can be discretized as follows:

$$\hat{a}(t) = q(t, \boldsymbol{\alpha}) \sum_{i=1}^{n} s_i\left(t, \boldsymbol{\lambda}(t_i)\right) U_i \tag{9}$$

where the standard normal random variable U_i represents an impulse at instant $t_i = i \times \dfrac{T}{n}$, $i = 1, \ldots, n$, (T is the total duration) and $s_i(t, \boldsymbol{\lambda}(t_i))$ is given by:

$$s_i(t, \boldsymbol{\lambda}(t_i)) = \frac{h\left[t - t_i, \boldsymbol{\lambda}(t_i)\right]}{\sqrt{\sum_{j=1}^{i} h^2\left[t - t_j, \boldsymbol{\lambda}(t_j)\right]}} \tag{10}$$

As a summary, the considered seismic generation model consists of three temporal parameters $(\alpha_1, \alpha_2, \alpha_3)$, three spectral parameters $(\omega_{mid}, \omega', \zeta_f)$ and the standard Gaussian random vector $\boldsymbol{U}$ of size n. Note that the full model proposed by [31] includes some additional parameters that are related to earthquake and site characteristics, *e.g.* the type of faulting of the earthquake (strike-slip fault or reverse fault), the closest distance from the recording site to the ruptured area and the shear-wave velocity of the top 30 m of the site soil. A methodology for determining the temporal and spectral parameters according to earthquake and site characteristics is described in [31]. For the sake of simplicity, in this paper these parameters are directly generated from appropriate statistical models.

3. Computation of fragility curves

Fragility curves represent the probability of failure of the system associated with a specified criterion for a given intensity measure (IM) of the earthquake motion. Herein probabilities of failure represent probabilities of exceeding demand limit states. The engineering demand parameter typically used for buildings is the maximal inter-storey drift ratio Δ, *i.e.* the maximal difference of horizontal displacements between consecutive storeys normalized by the storey height [6]. Thus the fragility curve is cast as follows:

$$\mathrm{Frag}(IM;\, \delta_o) = \mathbb{P}[\Delta \geq \delta_o | IM] \tag{11}$$

in which $\mathrm{Frag}(IM;\, \delta_o)$ denotes the fragility at the given IM for a prescribed demand threshold δ_o of the inter-storey drift ratio. In order to establish the fragility curves, a number N of transient finite element analyses of the structure under consideration are used to provide paired values $\{(IM_i, \Delta_i)\,, i = 1,\, \ldots\,, N\}$.

3.1. Classical approach

The classical approach to establish fragility curves consists in assuming a *lognormal shape* for the curves in Eq. (11). Two techniques are commonly used to estimate the parameters of the lognormal fragility curves, namely maximum likelihood estimation (MLE) and linear regression.

3.1.1. Maximum likelihood estimation:

One assumes that the fragility curves can be written in the following general form:

$$\widehat{\mathrm{Frag}}(IM;\, \delta_o) = \Phi\left(\frac{\log IM - \log \alpha}{\beta}\right) \tag{12}$$

where $\Phi\,(t) = \int\limits_{-\infty}^{t} e^{-u^2/2}/\sqrt{2\pi}\mathrm{d}u$ is the standard Gaussian cumulative distribution function (CDF), α is the "median" and β is the "log-standard deviation" of the lognormal curve. [21] proposed the use of maximum likelihood estimation to determine these parameters as follows: Denote by ω the event that the demand threshold δ_o is reached or exceeded. Assume that $Y(\omega)$ is a random variable with Bernoulli distribution, *i.e.* Y takes the value 1 (resp.

0) with probability $\text{Frag}(\cdot;\, \delta_o)$ (resp. $1 - \text{Frag}(\cdot;\, \delta_o)$). Considering a set of $i = 1, \ldots, N$ ground motions, the likelihood function reads:

$$\mathcal{L}\left(\alpha,\, \beta,\, \{IM_i,\, i = 1, \ldots, N\}\right) = \prod_{i=1}^{N} \left[\text{Frag}(IM_i;\, \delta_o)\right]^{y_i} \left[1 - \text{Frag}(IM_i;\, \delta_o)\right]^{1-y_i} \tag{13}$$

where IM_i is the intensity measure of the i^{th} seismic motion and y_i represents a realization of the Bernoulli random variable Y, which takes the value 1 or 0 depending on whether the structure under the i^{th} ground motion sustains the demand threshold δ_o or not. The parameters $(\alpha,\, \beta)$ are obtained by maximizing the likelihood function. In practice, a straightforward optimization algorithm is applied on the log-likelihood function, *i.e.* :

$$\{\alpha^*;\, \beta^*\}^{\mathsf{T}} = \arg\max \log \mathcal{L}\left(\alpha,\, \beta,\, \{IM_i,\, i = 1, \ldots, N\}\right) \tag{14}$$

3.1.2. Linear regression:

One first assumes a *probabilistic seismic demand model* which relates a structural response quantity to an intensity measure of the earthquake motion. More specifically, the maximal inter-storey drift Δ is modelled by a lognormal distribution whose log-mean value is a *linear function* of $\log IM$:

$$\log \Delta = A\, \log IM + B + \zeta\, Z \tag{15}$$

where $Z \sim \mathcal{N}(0, 1)$ is a standard normal variable. Parameters A and B are determined by means of ordinary least squares estimation in a log-log plot. This approach is widely applied in the literature, see *e.g.* [22, 29, 32, 33] among others. The procedure is based on the assumed linear relationship between IM and Δ in the log-scale. Let us denote by e_i the residual between the actual value $\log \Delta$ and the value predicted by the linear model: $e_i = \log \Delta_i - A \log\left(IM_i\right) - B$. Parameter ζ is obtained by:

$$\zeta^2 = \sum_{i=1}^{N} e_i^2 / \left(N - 2\right) \tag{16}$$

Eq. (11) rewrites:

$$\begin{aligned} \widehat{\text{Frag}}(IM;\, \delta_o) &= \mathbb{P}\left[\log \Delta \geq \log \delta_o\right] = 1 - \mathbb{P}\left[\log \Delta \leq \log \delta_o\right] \\ &= \Phi\left(\frac{\log IM - \left(\log \delta_o - B\right)/A}{\zeta / A}\right) \end{aligned} \tag{17}$$

The median and log-standard deviation of the lognormal fragility curve in Eq. (17) are $\alpha = \exp\left[\left(\log \delta_o - B\right)/A\right]$ and $\beta = \zeta/A$ respectively.

The above so-called classical approach is *parametric* because it imposes the shape of the fragility curves in Eq. (12) and Eq. (17) which is similar to a lognormal CDF when considered as a function of IM. In the sequel, we propose two *non-parametric* approaches to compute fragility curves *without* making such an assumption.

3.2. Binned Monte Carlo simulation

Having at hand a large sample set of pairs $\{(IM_j, \Delta_j)\,,\, j = 1, \ldots, N\}$, it is possible to use a *binned Monte Carlo simulation* (bMCS) to compute the fragility curves, as described in the following. Let us consider a given abscissa IM_o. Within a small bin surrounding IM_o, say $[IM_o - h, IM_o + h]$ (see Figure 1) one assumes that the maximal drift Δ is linearly related to the IM. Note that this assumption is exact in the case of linear structures but would only be an approximation in the nonlinear case. Therefore, the maximal drift Δ_j related to $IM_j \in [IM_o - h, IM_o + h]$ is converted into the drift $\Delta_j(IM_o)$ which is related to a similar input signal having an intensity measure of IM_o as follows:

$$\Delta_j(IM_o) = \Delta_j \frac{IM_o}{IM_j} \tag{18}$$

The fragility curve at IM_o is obtained by a crude Monte Carlo estimator:

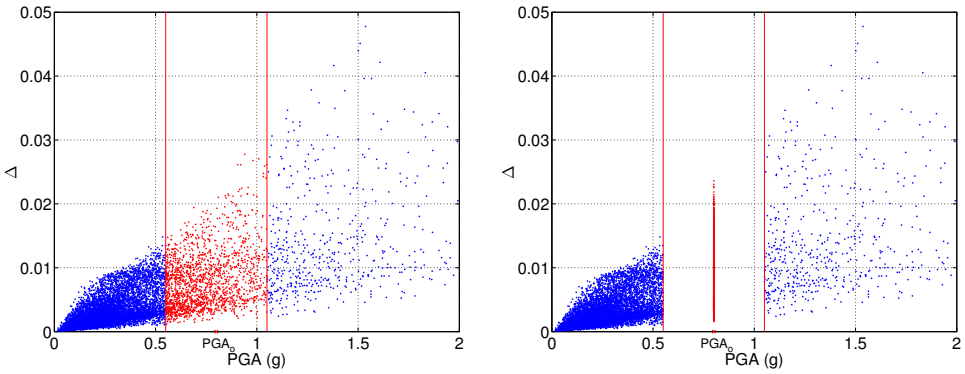


Figure 1: Scaling of ground motions and corresponding responses in the binned Monte Carlo simulation approach (the bin is enlarged for the sake of clarity).

$$\widehat{\mathrm{Frag}}(IM_o) = \frac{N_f\,(IM_o)}{N_s\,(IM_o)} \tag{19}$$

where $N_f\,(IM_o)$ is the number of points in the bin such that $\Delta_j(IM_o) \geqslant \delta_o$ and $N_s(IM_o)$ is the total number of points that fall into the bin $[IM_o - h, IM_o + h]$.

The bMCS approach is similar to the incremental dynamic analysis (IDA) in [34, 35, 36] except that when using IDA, one scales *all* the ground motions to the intensity level of interest. Therefore in the IDA approach there are signals scaled with very large (or very small) scale factors compared to unity which may lead to a gross approximation of the corresponding responses [37, 38]. Figure 2 shows the bias ratios induced by the scaling of ground motions for two different intensity measures. The bias for a certain scale factor is represented by the ratio of the mean maximal displacement response of a nonlinear SDOF system subject to the scaled motions to the respective response of the system without scaling of the motions. Note that the bias ratio becomes larger with increasing deviation of the scale factor from unity. In our approach, Eq. (18) basically represents the scaling of the ground motions in the vicinity of the intensity level IM_o. The vicinity is defined by the bin width $2h$ which is chosen so that the scale factors are close to 1 and typically in the range [0.8, 1.2] as in the application in Section 4. Accordingly, the bias due to ground motion scaling is negligible.

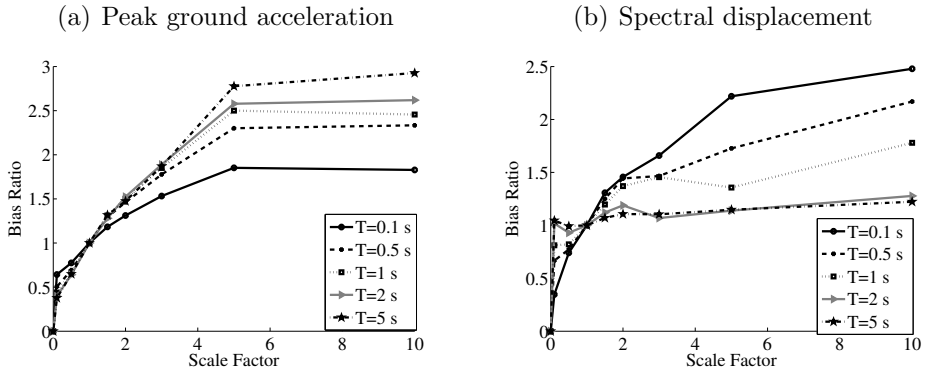


Figure 2: Bias ratios induced by the scaling of ground motions for two different intensity measures, namely peak ground acceleration and spectral displacement (after [37]).

3.3. Kernel density estimation

The fragility curves defined in Eq. (11) may be reformulated using the conditional probability density function (PDF) $f_{\Delta|IM}$ as follows:

$$\mathrm{Frag}(a;\, \delta_o) = \mathbb{P}\left(\Delta \geq \delta_o | IM = a\right) = \int_{\delta_o}^{+\infty} f_{\Delta}(\delta | IM = a)\, \mathrm{d}\delta \tag{20}$$

By definition this conditional PDF is given as:

$$f_{\Delta}(\delta | IM = a) = \frac{f_{\Delta, IM}(\delta, a)}{f_{IM}(a)} \tag{21}$$

where $f_{\Delta,IM}(\cdot)$ (resp. $f_{IM}(\cdot)$) is the joint distribution of the vector (Δ, IM) (resp. the marginal distribution of IM). If these quantities were known, the fragility curve in Eq. (20) would be obtained by a mere integration.

In this section we propose to *estimate* the joint and marginal PDFs from a sample set $\{(IM_i, \Delta_i),\, i = 1, \ldots, N\}$ by *kernel density estimation* (KDE). For a single random variable X for which a sample set $\{x_1, \ldots, x_N\}$ is available, the kernel density estimate of the PDF reads [39]:

$$\hat{f}_X\left(x\right) = \frac{1}{Nh} \sum_{i=1}^{N} K\left(\frac{x - x_i}{h}\right) \tag{22}$$

where h is the *bandwidth* parameter and $K(\cdot)$ is the *kernel* function which integrates to one. Classical kernel functions are the Epanechnikov, uniform, normal and triangular functions. The choice of the kernel is known not to affect strongly the quality of the estimate [39] provided the sample set is large enough. In case a standard normal PDF is adopted for the kernel, *i.e.* $K(x) = \varphi(x) \equiv \exp\left[-x^2/2\right]/\sqrt{2\pi}$, the kernel density estimate rewrites:

$$\hat{f}_X\left(x\right) = \frac{1}{Nh} \sum_{i=1}^{N} \varphi\left(\frac{x - x_i}{h}\right) \tag{23}$$

In contrast, the choice of the bandwidth h is crucial for the kernel density estimate [40]. An inappropriate value of h can lead to an oversmoothed or undersmoothed estimated PDF. Eq. (23) is used for estimating the marginal

distribution of the IMs, namely $\hat{f}_{IM}(a)$ from the set of intensity measures at hand, namely $\{IM_i,\, i = 1,\, \ldots\, , N\}$:

$$\hat{f}_{IM}(a) = \frac{1}{N h_{IM}} \sum_{i=1}^{N} \varphi\left(\frac{a - IM_i}{h_{IM}}\right) \tag{24}$$

Kernel density estimation may be extended to a random vector $\boldsymbol{X} \in \mathbb{R}^d$ given an i.i.d sample $\{\boldsymbol{x}_1,\, \ldots\, , \boldsymbol{x}_N\}$ [39]:

$$\hat{f}_{\boldsymbol{X}}\left(\boldsymbol{x}\right) = \frac{1}{N\left|\boldsymbol{H}\right|^{1/2}} \sum_{i=1}^{N} K\left(\boldsymbol{H}^{-1/2}(\boldsymbol{x} - \boldsymbol{x}_i)\right) \tag{25}$$

in which $\boldsymbol{H}$ is a symmetric positive definite *bandwidth matrix* whose determinant is denoted by $|\boldsymbol{H}|$. When a multivariate standard normal kernel is adopted, the joint distribution estimate becomes:

$$\hat{f}_{\boldsymbol{X}}\left(\boldsymbol{x}\right) = \frac{1}{N\left|\boldsymbol{H}\right|^{1/2}} \sum_{i=1}^{N} \frac{1}{(2\pi)^{d/2}} \exp\left[-\frac{1}{2}(\boldsymbol{x} - \boldsymbol{x}_i)^{\mathsf{T}} \boldsymbol{H}^{-1}(\boldsymbol{x} - \boldsymbol{x}_i)\right] \tag{26}$$

where $(\cdot)^{\mathsf{T}}$ denotes the transposition. For multivariate problems (*i.e.* $\boldsymbol{X} \in \mathbb{R}^d$), the bandwidth matrix classically belongs to one of the following classes: spherical, ellipsoidal and full matrix which contains respectively 1, d and $d(d+1)/2$ independent unknown parameters. This matrix $\boldsymbol{H}$ can be computed by means of *e.g.* plug-in and cross-validation estimators (see [40] for details). In the most general case when the correlations between the random variables are not known, the full matrix should be used. In this case, the *smoothed cross-validation estimator* is the most reliable among the cross-validation methods [41]. Using Eq. (26) to estimate the joint PDF $\hat{f}_{\Delta,IM}(\delta, a)$ from the data set $\{(IM_i,\, \Delta_i),\, i = 1,\, \ldots\, , N\}$ one gets:

$$\hat{f}_{\Delta,IM}(\delta, a) = \frac{1}{2\pi N\left|\boldsymbol{H}\right|^{1/2}} \sum_{i=1}^{N} \exp\left[-\frac{1}{2}\begin{pmatrix}\delta - \Delta_i \\ a - IM_i\end{pmatrix}^{\mathsf{T}} \boldsymbol{H}^{-1} \begin{pmatrix}\delta - \Delta_i \\ a - IM_i\end{pmatrix}\right] \tag{27}$$

The conditional PDF $f_{\Delta}(\delta|IM = a)$ is eventually estimated by pluging the estimations of the numerator and denominator in Eq. (21). The proposed

estimator of the fragility curve eventually reads:

$$\widehat{\mathrm{Frag}}(a;\,\delta_o) = \frac{h_{IM}}{2\pi\,|\boldsymbol{H}|^{1/2}} \frac{\int_{\delta_o}^{+\infty} \sum_{i=1}^{N} \exp\left[-\frac{1}{2}\begin{pmatrix}\delta-\Delta_i\\ a-IM_i\end{pmatrix}^{\mathsf{T}} \boldsymbol{H}^{-1} \begin{pmatrix}\delta-\Delta_i\\ a-IM_i\end{pmatrix}\right] \mathrm{d}\delta}{\sum_{i=1}^{N} \varphi\left(\frac{a-IM_i}{h_{IM}}\right)} \tag{28}$$

The choice of the bandwidth parameter h and the bandwidth matrix $\boldsymbol{H}$ plays a crucial role in the estimation of fragility curves, as seen in Eq. (28). In the above formulation, the same bandwidth is considered for the whole range of the IM values. However, there are typically few observations corresponding to the upper tail of the distribution of IM. This is due to the fact that the annual frequency of seismic motions with IM values in the respective range (*e.g.* PGA exceeding $1g$) is low (see *e.g.* [42]). This is also the case when synthetic ground motions are used, since these are generated consistently with the statistical features of recorded motions. Preliminary investigations have shown that by applying the KDE method on the data in the original scale, the fragility curves for the higher demand thresholds tend to be unstable in their upper tails [43]. To reduce effects of the scarcity of observations at large IM values, we propose the use of KDE in the logarithmic scale, as described next.

Let us consider two random variables X, Y with positive supports and their logarithmic transformations $U = \log X$ and $V = \log Y$. The probability contained in a differential area must be invariant under the change of variables. In the one-dimensional case, this leads to:

$$f_X(x) = \left|\frac{\mathrm{d}u}{\mathrm{d}x}\right| f_U(U) = \left|\frac{1}{x}\right| f_U(u) = \frac{1}{x} f_U(u) \tag{29}$$

In the two-dimensional case, one obtains:

$$f_{X,Y}(x,y) = \frac{1}{x\,y} f_{U,V}(u,v) \tag{30}$$

Using Equations (29) and (30), one has:

$$\int_{y_0}^{+\infty} f_Y(y|X=x)\,\mathrm{d}y = \int_{y_0}^{+\infty} \frac{f_{X,Y}(x,y)}{f_X(x)}\,\mathrm{d}y = \int_{\log y_0}^{+\infty} \frac{\frac{1}{x\,y} f_{U,V}(u,v)}{\frac{1}{x} f_U(u)}\, y\,\mathrm{d}v = \int_{\log y_0}^{+\infty} f_V(v|U=u)\,\mathrm{d}v \tag{31}$$

Accordingly, by considering $X = IM$ and $Y = \Delta$, the fragility curves defined in Eq. (20) can be estimated in terms of $U = \log IM$ and $V = \log \Delta$ as:

$$\widehat{\mathrm{Frag}}(a;\, \delta_o) = \int_{\delta_o}^{+\infty} \hat{f}_{\Delta}(\delta | IM = a)\, \mathrm{d}\delta = \int_{\log \delta_o}^{+\infty} \hat{f}_{V}(v | U = \log a)\, \mathrm{d}v \tag{32}$$

Note that use of a constant bandwidth in the logarithmic scale is equivalent to the use of a varying bandwidth in the original scale, with larger bandwidths corresponding to larger values of IM. The resulting fragility curves are smoother than those obtained by applying KDE with the data in the original scale.

3.4. Epistemic uncertainty of fragility curves

It is of utmost importance in fragility analysis to investigate the variability in the estimated curves arising due to epistemic uncertainty. This is because any fragility curve is always computed based on a limited amount of data, *i.e.* a limited number of ground motions and related structural analyses. Large epistemic uncertainties may affect significantly the total variability of the seismic risk assessment outcomes. Consequently, characterizing and propagating epistemic uncertainties in seismic loss estimation has attracted attention from several researchers [2, 44, 45].

The theoretical approach to determine the variability of an estimator relies on repeating the estimation with an ensemble of different random samples. However, this approach is not feasible in earthquake engineering because of the high computational cost. In this context, the *bootstrap resampling* technique [46] is deemed appropriate [2]. Given a set of observations $\boldsymbol{X} = (X_1, \ldots, X_n)$ from an unspecified probability distribution F, the bootstrap method allows estimation of the statistics of a random variable that depends on both $\boldsymbol{X}$ and F in terms of the observed data $\boldsymbol{X}$ and their empirical distribution.

To estimate statistics of the fragility curves with the bootstrap method, we first draw M independent random samples *with replacement* from the original data set $\{(IM_i, \Delta_i)\, , i = 1, \ldots, N\}$. These represent the so-called bootstrap samples. Each bootstrap sample has the same size N as the original sample, but the observations are different: in a particular sample, some of the original observations may appear multiple times while others may be missing. Next, we compute the fragility curves for each bootstrap sample

using the approaches in Sections 3.1, 3.2 and 3.3. Finally, we perform statistical analysis of the so-obtained M bootstrap curves. In the subsequent example illustration, the above procedure is employed to evaluate the median and 95% confidence intervals of the estimated fragility curves and also, to assess the variability in the IM value corresponding to a 50% probability of failure.

In the following, the proposed non-parametric approaches, namely bMCS and KDE, as well as the classical lognormal approach for estimation of fragility curves are demonstrated in an example application on a frame structure. The uncertainty in the estimation of the bMCS- and KDE-based curves is also investigated.

4. Illustration: steel frame structure

4.1. Problem statement: 3-storey 3-span steel frame

We evaluate the fragility curves of a 3-storey 3-span steel frame structure with the following dimensions: storey-height $H = 3$ m, span-length $L = 5$ m (see Figure 3). The steel material has nonlinear isotropic hardening behavior following the uniaxial Giuffre-Menegotto-Pinto steel model as implemented in the finite element software OpenSees [47]. [5] have shown that uncertainty in the properties of the steel material has a negligible effect on seismic fragility curves. Therefore, mean material properties are employed in the subsequent fragility analysis. In particular, the properties considered are $E_0 = 210,000$ MPa for the Young's modulus, $f_y = 264$ MPa for the yield strength [48, 49] and $b = 0.01$ for the strain hardening ratio (ratio of the post-yield tangent to the initial value). Figure 3 depicts the hysteretic behavior of the steel material at a section of the frame for an example ground motion. The structural components are modelled with nonlinear elements with distributed plasticity along their lengths. The use of fiber sections allows modelling the plasticity over the element cross-sections [50]. The vertical load consists of dead-load (from the frame elements as well as the supported floors), and live load in accordance with Eurocode 1 [51] which result in a total distributed load on the beams $q = 20$ kN/m. The preliminary design is performed using the vertical loads to provide the necessary sections of columns and beams. The standard European I beams with designation IPE 300 R and IPE 330 R are chosen respectively for beams and columns. The dimensions of the sections are depicted in Figure 4. The first two natural periods (resp. frequencies) of the building obtained by modal analysis

of the corresponding linear model are $T_1 = 0.42$ s and $T_2 = 0.13$ s (resp. $f_1 = 2.38$ Hz and $f_2 = 8.33$ Hz).

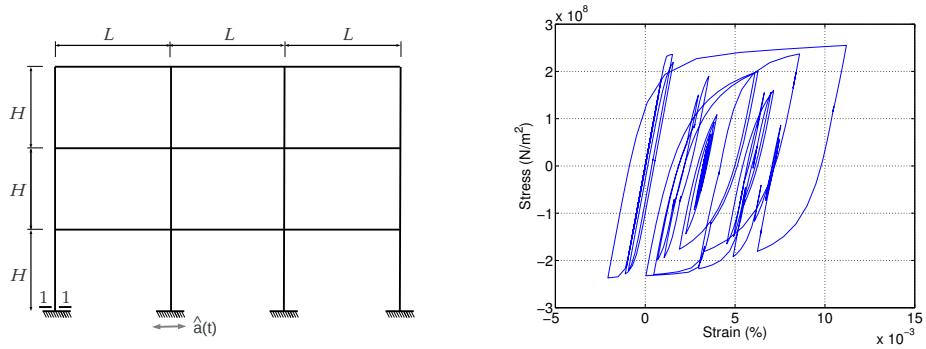


Figure 3: (Left) Steel frame structure. (Right) Hysteretic behavior of steel material at section 1-1 when the frame is subject to a particular ground motion.

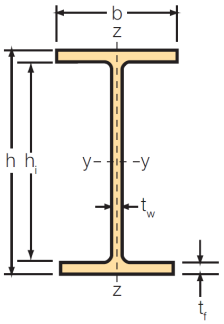


Figure 4: Cross-sections of beams (h=306 mm, b=147 mm, t_w=8,5 mm, t_f=13,7 mm) and columns (h = 336 mm, b=158 mm, t_w=9,2 mm, t_f=14,5 mm).

The structure is subject to ground motions represented by the acceleration time histories at the ground level. Each ground motion is modelled by 6 randomized parameters $(\alpha_1, \alpha_2, \alpha_3, \omega_{mid}, \omega', \zeta_f)$ directly related to the parameters in Table 1 and a Gaussian input vector $\boldsymbol{U}$ (Eq. (9)). The reader is referred to [31] for viewing the correlation between these parameters. Note that in order to obtain a sufficiently wide range of IM, we adapted the statistics of I_a, D_{5-95} and t_{mid} presented in [31]. The duration of each synthetic earthquake is computed based on the corresponding set of parameters $(\alpha_1, \alpha_2, \alpha_3)$ and is used to determine the size of the Gaussian vector $\boldsymbol{U}$. A

set of four different synthetic ground motions is shown in Figure 5 for the sake of illustration. The finite element code OpenSees [47] is used to carry out transient dynamic analyses of the frame for a total of $N = 10^4$ synthetic ground motions.

Numerous IMs can be used to represent the earthquake severity, see *e.g.* [52]. Peak ground acceleration (PGA) is a convenient measure that is straightforward to obtain for a given ground motion and has been traditionally used in attenuation relationships and design codes. However, structural responses may exhibit large dispersions with respect to PGA, since they are also highly dependent on other features of earthquake motions, e.g. the frequency content and the duration of the strong motion phase. Structure-specific IMs, such as the spectral acceleration Sa, tend to be better correlated with structural responses [52, 53]. In the following, we compute fragility curves considering both PGA and Sa as IMs. In the present example, Sa represents $Sa(T_1)$ *i.e.* the spectral acceleration for a SDOF system with period equal to the fundamental period T_1 of the frame and viscous damping factor equal 5%.

The engineering demand parameter commonly considered in fragility analysis of steel buildings is the inter-storey drift ratio (see *e.g.* [5, 54, 55]). Accordingly, we herein develop fragility curves for three different thresholds of the maximum inter-storey drift ratio over the building. To gain insight into structural performance, we consider the thresholds 0.7%, 1.5% and 2.5%, which are associated with different damage states in seismic codes. In particular, the thresholds 0.7% and 2.5% are recommended by [56] to respectively characterize light damage and moderate damage for steel frames. The drift threshold 1.5% corresponds to the damage limitation requirement for buildings with ductile non-structural elements according to [57]. These descriptions only serve as rough damage indicators herein, since in the PBEE framework the relationship between drift limit and damage is probabilistic.

4.2. Results

As described in Section 3, the lognormal approach consists in assuming that the fragility curves have the shape of a lognormal CDF and then estimating the parameters of the distribution. Using the MLE approach, the observed failures for each drift threshold are modeled as outcomes of a Bernoulli experiment and the parameters of the fragility curves are determined by maximizing the respective likelihood function. Using the linear regression technique, the parameters of the lognormal curves are indirectly derived by

Table 1: Statistics of parameters used to generate the synthetic ground motions (adapted from [31]).

Parameter	Distribution	Support	μ_X	σ_X
I_a	Lognormal	$(0, +\infty)$	5.613	10.486
D_{5-95}	Beta	[5, 20]	10	2
t_{mid}	Beta	[5, 15]	12	2
ω_{mid} / 2π	Gamma	$(0, +\infty)$	5.930	3.180
ω' / 2π	Two-sided exponential	[-2, 0.5]	-0.089	0.185
ζ_f	Beta	[0.02, 1]	0.210	0.150

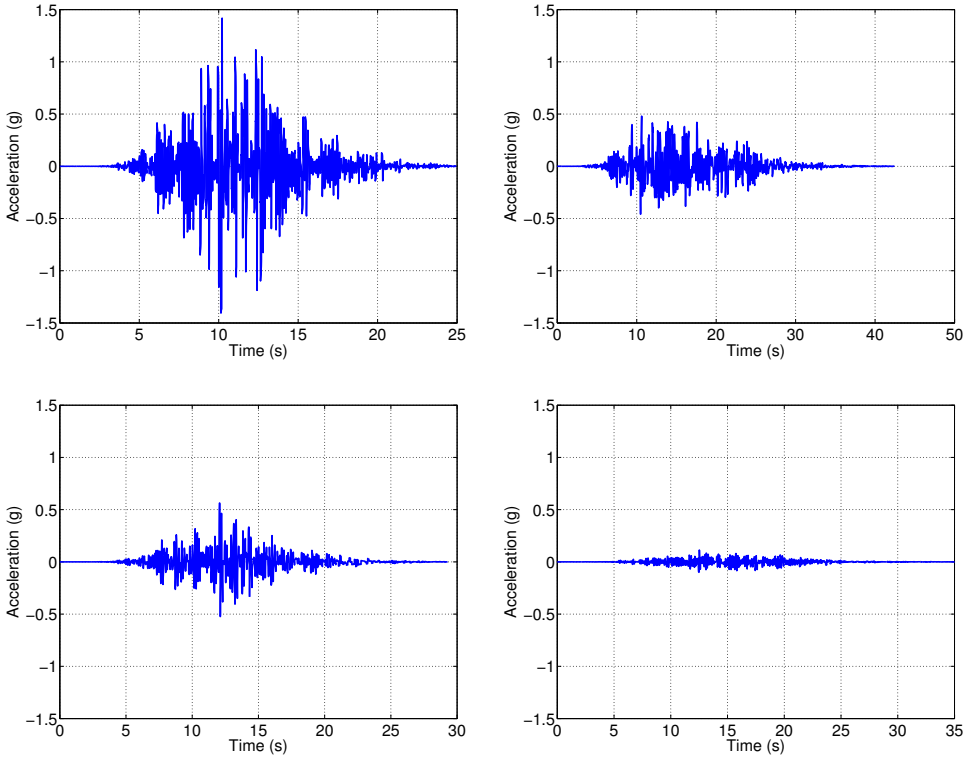


Figure 5: Examples of generated synthetic ground motions.

fitting a linear model to the paired data ($\log IM$, $\log \Delta$). Figure 6 (resp. Fig-

ure 7) depicts the paired data ($\log PGA$, $\log \Delta$) (resp. ($\log Sa$, $\log \Delta$)) and the fitted PSDM using linear regression. The coefficient of determination R^2 of the linear regression model considering PGA (resp. Sa) as an intensity measure is 0.607 (resp. 0.866). We observe that using Sa as an intensity measure leads to smaller dispersion *i.e.* smaller ζ in Eq. (15) as compared to using PGA. This is expected since Sa is a structure-specific IM. In the bMCS method, the bandwidth h is set equal to $0.2\,IM_o$. The resulting scale factors vary in the range [0.8, 1.2] yielding a bias ratio of approximately 1 (see Figure 2). Finally, the KDE approach requires estimation of the bandwidth parameter and the bandwidth matrix. Using the smoothed cross-validation estimation implemented in `R` [58], these are determined as $h = 0.1295$ and $\boldsymbol{H} = \begin{bmatrix} 0.0306 & 0.0246 \\ 0.0246 & 0.0283 \end{bmatrix}$ (resp. $h = 0.1441$ and $\boldsymbol{H} = \begin{bmatrix} 0.0229 & 0.0224 \\ 0.0224 & 0.0248 \end{bmatrix}$) when PGA (resp. Sa) is considered as IM.

For the two considered IMs and the three drift limits of interest, Table 2 lists the medians and log-standard deviations of the lognormal curves obtained with both the MLE and linear regression (LR) approaches. The median determines the position where the curve attains the value 0.5, whereas the log-standard deviation is a measure of the steepness of the curve. The medians of the KDE-based curves have been computed and are also listed in Table 2 for comparison. Larger deviations of the lognormal medians from the reference KDE-based values are observed at the larger drift thresholds for both parametric approaches. Note that the MLE approach yields a distinct log-standard deviation for each drift threshold, whereas a single log-standard deviation for all drift thresholds is obtained with the linear regression approach. The standard deviations obtained with MLE may be smaller or larger than those obtained with linear regression depending on the considered IM and threshold.

For the three considered drift thresholds, Figure 8 shows the lognormal (with two estimation approaches) and non-parametric (both bMCS- and KDE-based) fragility curves when PGA is used as IM. One first observes a remarkable consistency between the curves obtained with the two proposed non-parametric approaches for all limit states although the algorithms behind the methods are totally different. This validates the accuracy of the proposed approaches. For high values of PGA ($> 2\,g$), some noise is observed on the bMCS curves due to the scarcity of observations in the corresponding intervals. This noise may be reduced by using additional observations in this range of PGA. Note, however, that the set of synthetic motions used in our analy-

Table 2: Steel frame structure - Parameters of the obtained fragility curves.

		PGA		Sa	
δ_o	Approach	Median	Log-std	Median	Log-std
0.7%	MLE	$0.6844\,g$	0.6306	$1.2327\,g$	0.2915
	LR	$0.7392\,g$	0.6260	$1.3529\,g$	0.3433
	KDE	$0.7\,g$		$1.2\,g$	
1.5%	MLE	$1.7437\,g$	0.5194	$3.4184\,g$	0.4327
	LR	$1.6222\,g$	0.6260	$2.8377\,g$	0.3433
	KDE	$1.8\,g$		$3.3\,g$	
2.5%	MLE	$2.4958\,g$	0.4631	$6.3357\,g$	0.3769
	LR	$2.7472\,g$	0.6260	$4.6621\,g$	0.3433
	KDE	$3.0\,g$		$5.6\,g$	

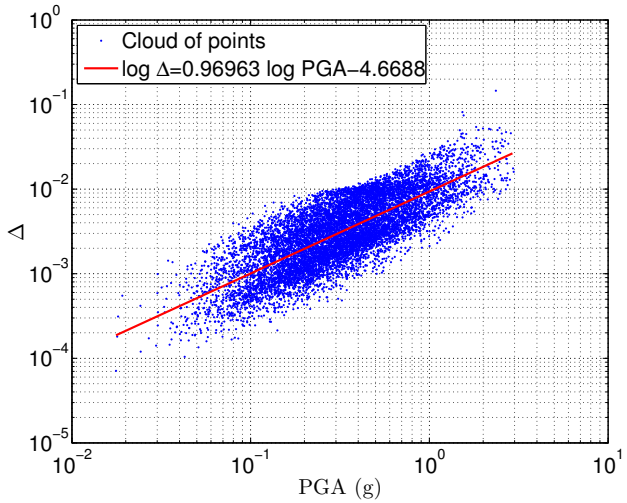


Figure 6: Paired data $\left\{(PGA_i, \Delta_i)\,, i = 1, \ldots, 10^4\right\}$ and linear regression in the logarithmic scale.

sis has statistical features characterizing the occurrence of actual earthquake motions (ground motions with large IMs have relatively low probabilities of occurrence). For the lower threshold ($\delta_o = 0.7\%$), the parametric curves are in fairly good agreement with the non-parametric curves. For the two higher thresholds, significant discrepancy is observed between the lognormal curves and the non-parametric ones. In particular, in the range of high PGA values, both lognormal curves overestimate the failure probabilities. It is noted that

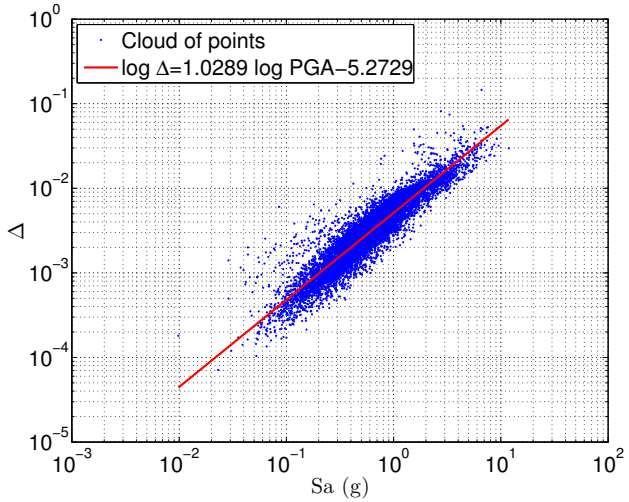


Figure 7: Paired data $\left\{(Sa_i, \Delta_i)\,, i = 1, \ldots, 10^4\right\}$ and linear regression in the logarithmic scale.

for $\delta_o = 2.5\%$, the median PGA (leading to 50% probability of exceedance) is respectively underestimated by 9% and 17% with the MLE and the linear regression aproach, respectively.

Figure 9 shows the resulting fragility curves when Sa is used as IM. The non-parametric curves by bMCS and KDE remain consistent independently of the limit state. For the two larger thresholds, the lognormal curves exhibit large variations from the non-parametric curves as well as between each other. In particular, the curves obtained with MLE underestimate moderate and large failure probabilities whereas the curves obtained with linear regression tend to overestimate failure probabilities. For $\delta_o = 2.5\%$, the median PGA is overestimated by 13% with the MLE approach and is underestimated by 17% with the linear regression approach. Note that by comparing the absolute discrepancies, linear regression estimation provides less accurate curves for Sa than for PGA, although the R^2 coefficient of the linear fit is higher for the former. This is due to the fact that the assumption of *normally distributed errors with constant variance*, which is inherent in Eq. (15), is not valid for Sa, as one observes in Figure 7. Under the assumption of a *unique linear model*, the median is overestimated at the lower drift limit and underestimated at the two larger drift limits.

The previous analysis shows that the two non-parametric approaches, namely bMCS and KDE, yield consistent fragility curves for both IMs and

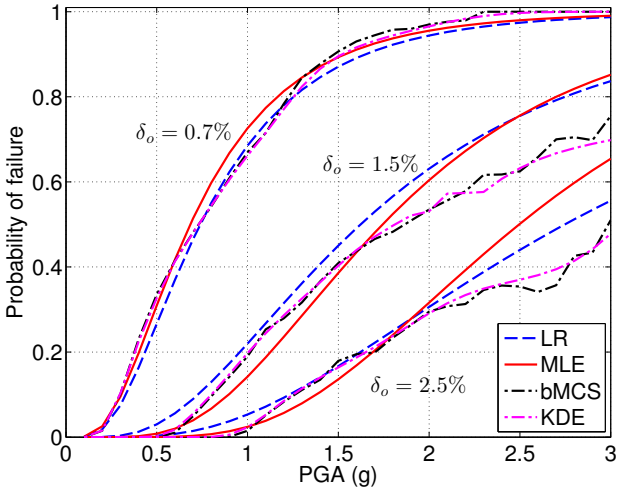


Figure 8: Fragility curves by parametric and non-parametric approaches using PGA as intensity measure. (LR: linear regression; MLE: maximum likelihood estimation; MCS: binned Monte Carlo simulation; KDE: kernel density estimation)

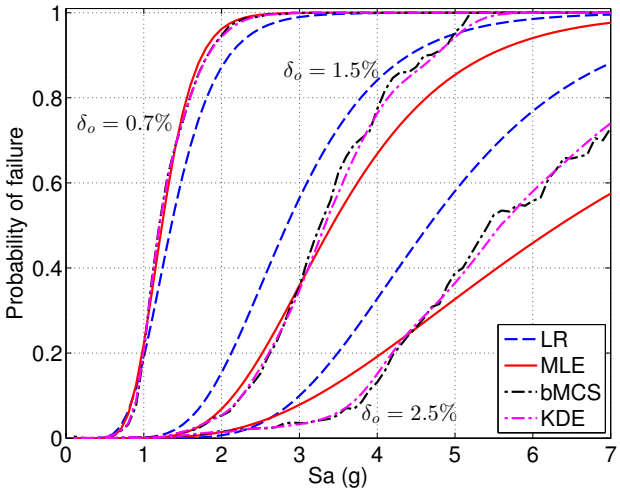


Figure 9: Fragility curves by parametric and non-parametric approaches using Sa as intensity measure. (LR: linear regression; MLE: maximum likelihood estimation; MCS: binned Monte Carlo simulation; KDE: kernel density estimation)

for all considered limit states. Using the non-parametric fragility curves as reference, the accuracy of the lognormal curves is found to depend strongly on the method for estimating the parameters of the underlying CDF, the

considered IM and the drift threshold of interest. Note that different IMs have been recommended in literature [53, 59] for structures of different type, size and material. Accordingly, the accuracy of the lognormal fragility curves may depend on those factors as well. Possible dependency of the accuracy of the lognormal curves on the considered response quantity also needs to be investigated.

4.3. Estimation of epistemic uncertainty by bootstrap resampling

In the following, we use the bootstrap resampling technique (see Section 3.4) to investigate the epistemic uncertainty in the fragility curves estimated with the proposed non-parametric approaches.

First, we examine the stability of the estimates by comparing those with the bootstrap medians, and the variability in the estimation by computing bootstrap confidence intervals. For the two considered IMs and the three limit states of interest, Figure 10 shows the median bMCS- and KDE-based fragility curves and the 95% confidence intervals obtained by bootstrap resampling with 100 replications. Figure 10 clearly shows that both the bMCS-based and the KDE-based median fragility curves obtained with the bootstrap method do not differ from the curves estimated with the original set of observations. This shows the stability of the proposed approaches. For a specified IM and drift limit, the confidence intervals of the bMCS- and KDE-based curves have similar widths. The interval widths tend to increase with increasing drift limit and increasing IM value. We note that for a certain drift limit and failure probability, the confidence intervals for the curves versus Sa tend to be narrower than for curves versus PGA. This is due to the higher correlation of structural responses with Sa.

In order to quantify the effect of epistemic uncertainty, one can assess the variability of the median IM, *i.e.* the IM value leading to 50% probability of exceedance. Assuming that the median IM (PGA or Sa) follows a lognormal distribution [60], the median IM is determined for each bootstrap curve and the log-standard deviation of the distribution of the median is computed. Table 3 lists the log-standard deviations of the median IM values for the same cases as in Figure 10. For the larger threshold $\delta_o = 2.5\%$ and PGA as IM, some curves did not reach probability of exceedance values as high as 50% and thus, results for this case are not shown. One observes in Table 3 that epistemic uncertainty is increasing with increasing threshold δ_o. For a certain threshold, using PGA as IM leads to a 4-5 times larger epistemic uncertainty compared to using Sa. Furthermore, log-standard deviations

of the median IMs are slightly smaller with the KDE approach than with the bMCS approach. However, in all cases, the log-standard deviations are small indicating a low level of epistemic uncertainty. This is due to the large number of ground motions ($N = 10^4$) considered in this study.

Table 3: Log-standard deviation of the median IM

δ_o	Approach	PGA	Sa
0.7%	bMCS	0.0289	0.0073
	KDE	0.0259	0.0052
1.5%	bMCS	0.0658	0.0168
	KDE	0.0639	0.0139
2.5%	bMCS		0.0493
	KDE		0.0306

5. Conclusions

Seismic demand fragility evaluation is one of the basic elements in the framework of performance-based earthquake engineering (PBEE). At present, the classical lognormal approach is widely used to establish such fragility curves mainly due to the fact that the lognormality assumption makes seismic risk analysis more tractable. The approach consists in assigning the shape of a lognormal cumulative distribution function to the fragility curves. However, the validity of this assumption remains an open question.

In this paper, we introduce two non-parametric approaches in order to examine the validity of the classical lognormal approach, namely the binned Monte Carlo simulation and the kernel density estimation. The former computes the crude Monte Carlo estimators for small subsets of ground motions with similar values of a selected intensity measure, while the latter estimates the conditional probability density function of the structural response given the ground motion intensity measures using the kernel density estimation technique. The proposed approaches can be used to compute fragility curves when the actual shape of these curves is not known as well as to validate or calibrate parametric fragility curves. Herein, the two non-parametric approaches are confronted to the classical lognormal approach on the example of a steel frame subject to synthetic ground motions.

(a) Binned Monte Carlo simulation (b) Kernel density estimation

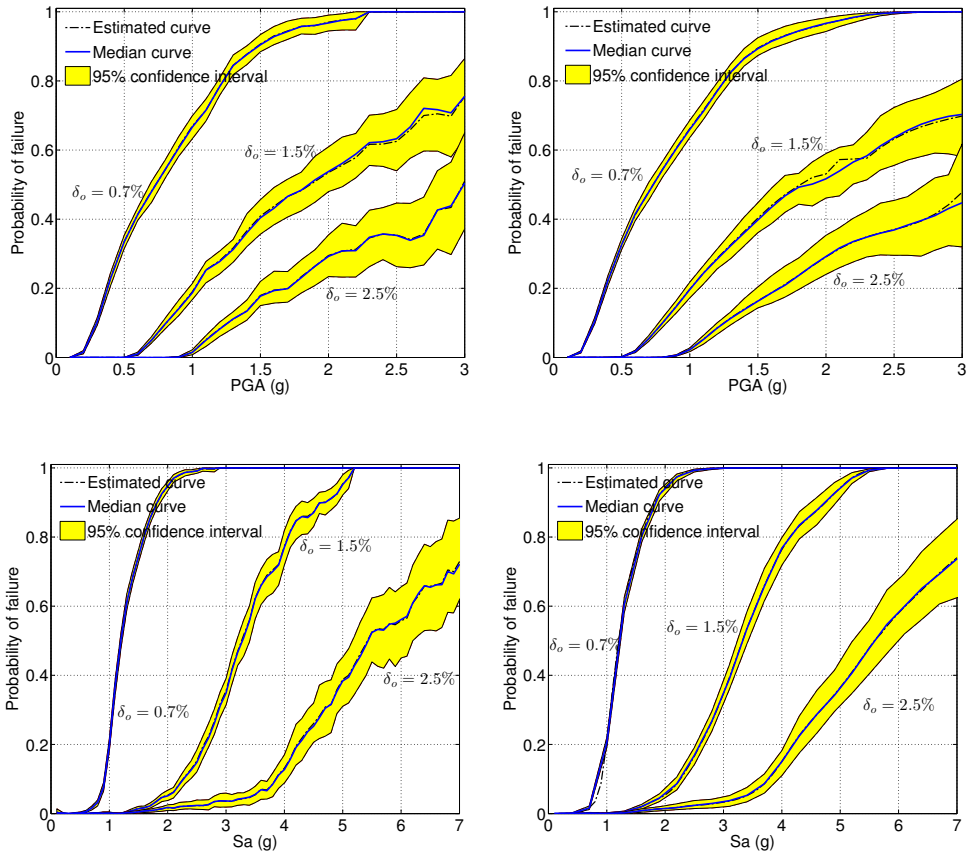


Figure 10: Estimated, mean bootstrap fragility curves and 95% confidence intervals by binned Monte Carlo simulation and kernel density estimation approaches. The mean curves and 95% confidence intervals are computed using bootstrap resampling technique with 100 replications.

In the case study, the fragility curves are established for three inter-storey drift-limit levels and two ground motion intensity measures, namely the peak ground acceleration (PGA) and the spectral acceleration (Sa). The two non-parametric curves are consistent in all cases which proves the validity of the proposed techniques. Accordingly, these are used as reference to assess the accuracy of the lognormal curves. The parameters of the latter are estimated with two approaches, namely by maximum likelihood estimation and by assuming a linear probabilistic seismic demand model in the log-scale. For

the two higher drift-limit levels, large discrepancies are observed between the non-parametric and the lognormal curves as well as between the two lognormal curves, which demonstrates the insufficiency of the parametric approach. Fragility estimates obtained with the latter may be conservative or not depending on the estimation approach, the intensity measure and the drift threshold. When integrated in the PBEE framework, the discrepancies of the lognormal curves from the "real" non-parametric ones may induce severe errors in the probabilistic consequence estimates that serve as decision variables for risk mitigation actions.

In the same case study, the bootstrap resampling technique is employed to assess effects of epistemic uncertainty in the non-parametric fragility curves. It is shown that for a certain limit state, epistemic uncertainty is lower for the case of Sa, which is a structure-specific intensity measure, than for the case of PGA. In addition, results from bootstrap analysis validate the stability of the fragility estimates with the proposed non-parametric methods.

Recently, fragility surfaces have emerged as an innovative way to represent the system's vulnerability [13] in which one calculates the failure probability conditional on two intensity measures of the earthquake motions. The computation of these surfaces is not straightforward and requires large computational effort. The present study opens new paths for establishing the fragility surfaces: similarly to the case of fragility curves, one can use kernel density estimation to obtain assumption-free fragility surfaces that are consistent with the true ones obtained by Monte Carlo simulation.

The computational cost of the two proposed approaches remains significant since they are based on rather large Monte Carlo samples. In order to reduce this cost, alternative approaches may be envisaged. Polynomial chaos (PC) expansions [61, 62] appear as a promising tool. Based on a smaller sample set (typically a few hundreds of finite element runs), PC expansion provides a polynomial approximation that surrogates the structural response. The feasibility of post-processing PC expansions in order to compute fragility curves has been shown in [63, 64] in the case a linear structural behavior is assumed. The extension to nonlinear behavior is currently in progress.

We underline that the proposed non-parametric approaches are essentially applicable to other probabilistic models in the PBEE framework, relating decision variables with structural damage and structural damage with structural response. Once all the non-parametric probabilistic models are available, they can be incorporated in the PBEE framework by means of numerical integration. Then a full seismic risk assessment may be conducted

by avoiding potential inaccuracies introduced from simplifying parametric assumptions at any step of the analysis. Optimal high-fidelity computational methods for incorporating non-parametric fragility curves in the PBEE framework will be investigated in the future.

References

[1] Porter KA. An overview of PEER's performance-based earthquake engineering methodology. In: Proc. 9th Int. Conf. on Applications of Stat. and Prob. in Civil Engineering (ICASP9), San Francisco. 2003, p. 6–9.

[2] Baker JW, Cornell CA. Uncertainty propagation in probabilistic seismic loss estimation. Structural Safety 2008;30(3):236–52.

[3] Günay S, Mosalam KM. PEER performance-based earthquake engineering methodology, revisited. J Earthq Eng 2013;17(6):829–58.

[4] Mackie K, Stojadinovic B. Fragility basis for California highway overpass bridge seismic decision making. Pacific Earthquake Engineering Research Center, College of Engineering, University of California, Berkeley; 2005.

[5] Ellingwood BR, Kinali K. Quantifying and communicating uncertainty in seismic risk assessment. Structural Safety 2009;31(2):179–87.

[6] Seo J, Duenas-Osorio L, Craig JI, Goodno BJ. Metamodel-based regional vulnerability estimate of irregular steel moment-frame structures subjected to earthquake events. Eng Struct 2012;45:585–97.

[7] Banerjee S, Shinozuka M. Nonlinear Static Procedure for Seismic Vulnerability Assessment of Bridges. Comput-Aided Civ Inf 2007;22(4):293–305.

[8] Richardson JE, Bagchi G, Brazee RJ. The seismic safety margins research program of the U.S. Nuclear Regulatory Commission. Nuc Eng Des 1980;59(1):15–25.

[9] Pei S, Van De Lindt J. Methodology for earthquake-induced loss estimation: An application to woodframe buildings. Structural Safety 2009;31(1):31–42.

[10] Eads L, Miranda E, Krawinkler H, Lignos DG. An efficient method for estimating the collapse risk of structures in seismic regions. Earthquake Eng Struct Dyn 2013;42(1):25–41.

[11] Dukes J, DesRoches R, Padgett JE. Sensitivity study of design parameters used to develop bridge specific fragility curves. In: Proc. 15th World Conf. Earthquake Eng. 2012,.

[12] Güneyisi EM, Altay G. Seismic fragility assessment of effectiveness of viscous dampers in R/C buildings under scenario earthquakes. Structural Safety 2008;30(5):461–80.

[13] Seyedi DM, Gehl P, Douglas J, Davenne L, Mezher N, Ghavamian S. Development of seismic fragility surfaces for reinforced concrete buildings by means of nonlinear time-history analysis. Earthquake Eng Struct Dyn 2010;39(1):91–108.

[14] Gardoni P, Der Kiureghian A, Mosalam KM. Probabilistic capacity models and fragility estimates for reinforced concrete columns based on experimental observations. J Eng Mech 2002;128(10):1024–38.

[15] Ghosh J, Padgett JE. Aging considerations in the development of time-dependent seismic fragility curves. J Struct Eng 2010;136(12):1497–511.

[16] Argyroudis S, Pitilakis K. Seismic fragility curves of shallow tunnels in alluvial deposits. Soil Dyn Earthq Eng 2012;35:1–12.

[17] Chiou J, Chiang C, Yang H, Hsu S. Developing fragility curves for a pile-supported wharf. Soil Dyn Earthq Eng 2011;31:830–40.

[18] Quilligan A, O Connor A, Pakrashi V. Fragility analysis of steel and concrete wind turbine towers. Engineering Structures 2012;36:270–82.

[19] Borgonovo E, Zentner I, Pellegri A, Tarantola S, de Rocquigny E. On the importance of uncertain factors in seismic fragility assessment. Reliab Eng Sys Safety 2013;109(0):66–76.

[20] Rossetto T, Elnashai A. A new analytical procedure for the derivation of displacement-based vulnerability curves for populations of RC structures. Engineering Structures 2005;27(3):397–409.

[21] Shinozuka M, Feng M, Lee J, Naganuma T. Statistical analysis of fragility curves. J Eng Mech 2000;126(12):1224–31.

[22] Ellingwood BR. Earthquake risk assessment of building structures. Reliab Eng Sys Safety 2001;74(3):251–62.

[23] Zentner I. Numerical computation of fragility curves for NPP equipment. Nuc Eng Des 2010;240:1614–21.

[24] Gencturk B, Elnashai A, Song J. Fragility relationships for populations of woodframe structures based on inelastic response. J Earthq Eng 2008;12:119–28.

[25] Jeong SH, Mwafy AM, Elnashai AS. Probabilistic seismic performance assessment of code-compliant multi-story RC buildings. Engineering Structures 2012;34:527–37.

[26] Banerjee S, Shinozuka M. Mechanistic quantification of RC bridge damage states under earthquake through fragility analysis. Prob Eng Mech 2008;23(1):12–22.

[27] Hwang HH, Huo JR. Generation of hazard-consistent fragility curves. Soil Dyn Earthq Eng 1994;13(5):345–54.

[28] Lupoi A, Franchin P, Pinto PE, Monti G. Seismic design of bridges accounting for spatial variability of ground motion. Earthquake Eng Struct Dyn 2005;34(4-5):327–48.

[29] Choi E, DesRoches R, Nielson B. Seismic fragility of typical bridges in moderate seismic zones. Eng Struct 2004;26(2):187–99.

[30] Rezaeian S, Der Kiureghian A. A stochastic ground motion model with separable temporal and spectral nonstationarities. Earthquake Eng Struct Dyn 2008;37(13):1565–84.

[31] Rezaeian S, Der Kiureghian A. Simulation of synthetic ground motions for specified earthquake and site characteristics. Earthquake Eng Struct Dyn 2010;39(10):1155–80.

[32] Padgett JE, DesRoches R. Methodology for the development of analytical fragility curves for retrofitted bridges. Earthquake Eng Struct Dyn 2008;37(8):1157–74.

[33] Zareian F, Krawinkler H. Assessment of probability of collapse and design for collapse safety. Earthquake Eng Struct Dyn 2007;36(13):1901–14.

[34] Vamvatsikos D, Cornell CA. Incremental dynamic analysis. Earthquake Eng Struct Dyn 2002;31(3):491–514.

[35] Vamvatsikos D, Cornell CA. Direct estimation of seismic demand and capacity of multidegree-of-freedom systems through Iincremental dynamic analysis of single degree of freedom approximation1. J Struct Eng 2005;131(4):589–99.

[36] Mander JB, Dhakal RP, Mashiko N, Solberg KM. Incremental dynamic analysis applied to seismic financial risk assessment of bridges. Eng Struct 2007;29(10):2662–72.

[37] Mehdizadeh M, Mackie KR, Nielson BG. Scaling bias and record selection for fragility analysis. In: Proc. 15th World Conf. Earthquake Eng. 2012,.

[38] Cimellaro GP, Reinhorn AM, D'Ambrisi A, De Stefano M. Fragility analysis and seismic record selection. J Struct Eng 2009;137(3):379–90.

[39] Wand M, Jones MC. Kernel smoothing. Chapman and Hall; 1995.

[40] Duong T. Bandwidth selectors for multivariate kernel density estimation. Ph.D. thesis; School of mathematics and Statistics, University of Western Australia; 2004.

[41] Duong T, Hazelton ML. Cross-validation bandwidth matrices for multivariate kernel density estimation. Scand J Stat 2005;32(3):485–506.

[42] Frankel AD, Mueller CS, Barnhard TP, Leyendecker EV, Wesson RL, Harmsen SC, et al. USGS national seismic hazard maps. Earthquake spectra 2000;16(1):1–19.

[43] Sudret B, Mai CV. Calcul des courbes de fragilité par approches non-paramétriques. In: Proc. 21e Congrès Français de Mécanique (CFM21), Bordeaux. 2013,.

[44] Bradley BA, Lee DS. Accuracy of approximate methods of uncertainty propagation in seismic loss estimation. Structural Safety 2010;32(1):13–24.

[45] Liel AB, Haselton CB, Deierlein GG, Baker JW. Incorporating modeling uncertainties in the assessment of seismic collapse risk of buildings. Structural Safety 2009;31(2):197–211.

[46] Efron B. Bootstrap methods: another look at the Jackknife. The annals of Statistics 1979;:1–26.

[47] Pacific Earthquake Engineering and Research Center . OpenSees: The Open System for Earthquake Engineering Simulation. 2004.

[48] Eurocode 3 . Design of steel structures - Part 1-1: General rules and rules for buildings. 2005.

[49] Joint Committee on Structural Safety . Probabilistic Model Code - Part 3 : Resistance Models. 2001.

[50] Deierlein GG, Reinhorn AM, Willford MR. Nonlinear structural analysis for seismic design. NEHRP Seismic Design Technical Brief No 2010;4.

[51] Eurocode 1 . Actions on structures - Part 1-1: general actions - densities, self-weight, imposed loads for buildings. 2004.

[52] Mackie K, Stojadinovic B. Improving probabilistic seismic demand models through refined intensity measures. In: Proc. 13th World Conf. Earthquake Eng. Int. Assoc. for Earthquake Eng. Japan; 2004,.

[53] Padgett J, Nielson B, DesRoches R. Selection of optimal intensity measures in probabilistic seismic demand models of highway bridge portfolios. Earthquake Eng Struct Dyn 2008;37(5):711–25.

[54] Cornell C, Jalayer F, Hamburger R, Foutch D. Probabilistic basis for 2000 SAC Federal Emergency Management Agency steel moment frame guidelines. J Struct Eng (ASCE) 2002;128(4):526–33.

[55] Lagaros ND, Fragiadakis M. Fragility sssessment of steel frames using neural networks. Earthquake Spectra 2007;23(4):735–52.

[56] Federal Emergency Management Agency, Washington, DC . Commentary for the seismic rehabilitation of buildings; 2000.

[57] Eurocode 8 . Design of structures for earthquake resistance - Part 1: General rules, seismic actions and rules for buildings; 2004.

[58] Duong T. ks: kernel density estimation and kernel discriminant analysis for multivariate data in R. J Stat Softw 2007;21(7):1–16.

[59] Jankovic S, Stojadinovic B. Probabilistic performance based seismic demand model for R/C frame buildings. In: Proc. 13th World Conf. Earthquake Eng. 2004,.

[60] Choun YS, Elnashai AS. A simplified framework for probabilistic earthquake loss estimation. Prob Eng Mech 2010;25(4):355–64.

[61] Ghanem R, Spanos P. Stochastic Finite Elements : A Spectral Approach. Courier Dover Publications; 2003.

[62] Blatman G, Sudret B. Adaptive sparse polynomial chaos expansion based on Least Angle Regression. J Comput Phys 2011;230:2345–67.

[63] Sudret B, Piquard V, Guyonnet C. Use of polynomial chaos expansions to establish fragility curves in seismic risk assessment. In: G. De Roeck G. Degrande GL, Müller G, editors. Proc. 8th Int. Conf. Struct. Dynamics (EURODYN 2011), Leuven, Belgium. 2011,.

[64] Sudret B, Mai CV. Computing seismic fragility curves using polynomial chaos expansions. In: Deodatis G, editor. Proc. 11th Int. Conf. Struct. Safety and Reliability (ICOSSAR'2013), New York, USA. 2013,.